

Correction

MICROBIOLOGY

Correction for “Integrative approach using *Yersinia pestis* genomes to revisit the historical landscape of plague during the Medieval Period,” by Amine Namouchi, Meriam Guellil, Oliver Kersten, Stephanie Hänsch, Claudio Ottoni, Boris V. Schmid, Elsa Pacciani, Luisa Quaglia, Marco Vermunt, Egil L. Bauer, Michael Derrick, Anne Ø. Jensen, Sacha Kacki, Samuel K. Cohn Jr., Nils C. Stenseth, and Barbara Bramanti, which was first published November 26, 2018; 10.1073/pnas.1812865115 (*Proc Natl Acad Sci USA* 115:E11790–E11797).

The editors note that the publication year for reference 28 appeared incorrectly. The reference should instead appear as: Carmichael AG (2014) Plague Persistence in Western Europe: A Hypothesis. *The Medieval Globe*: Vol 1, No 1, Article 8.

Published under the [PNAS license](#).

Published online December 24, 2018.

www.pnas.org/cgi/doi/10.1073/pnas.1820659116

Correction

MICROBIOLOGY

Correction for “Integrative approach using *Yersinia pestis* genomes to revisit the historical landscape of plague during the Medieval Period,” by Amine Namouchi, Meriam Guellil, Oliver Kersten, Stephanie Hänsch, Claudio Ottoni, Boris V. Schmid, Elsa Pacciani, Luisa Quaglia, Marco Vermunt, Egil L. Bauer, Michael Derrick, Anne Ø. Jensen, Sacha Kacki, Samuel K. Cohn Jr., Nils C. Stenseth, and Barbara Bramanti, which was first published November 26, 2018; 10.1073/pnas.1812865115 (*Proc. Natl. Acad. Sci. U.S.A.* **115**, E11790–E11797).

The authors wish to note, “Three passages within our *SI Appendix* were similar to those we used in an unpublished manuscript by Raffaella Bianucci, Stephanie Hänsch, Luisa Quaglia, Stelvio Mambrini, Elsa Pacciani, Samuel K. Cohn Jr., and Barbara Bramanti, which dealt with the plague epidemic at Abbadia San Salvatore. The passages in question, which appear in the *SI Appendix* of our article under the headings *History of plague in the abbey of San Salvatore*, *Archaeology and osteology of the abbey of San Salvatore*, and *Parchments of Monte Amiata*, contain archaeological and historical data independently contributed by Elsa Pacciani, Luisa Quaglia, and Samuel K. Cohn Jr., and used in two distinct projects resulting in the Bianucci et al. manuscript and in our PNAS article.

“We would like to update our acknowledgments to thank R. Bianucci for her initial involvement in the first project about Abbadia San Salvatore.

“Additionally, we would like to make the following updates to the sources and credits for three figures in our *SI Appendix*:”

Fig. S1. Map of the monastery in San Salvatore. The green area represents the burial area. The map was used also in a different picture of Bianucci et al., unpublished. Image credit: Luisa Quaglia and Elsa Pacciani.

Fig. S2. Two examples of burials excavated at the abbey of San Salvatore, with longitudinal ditches intersected by later depositions. The picture on the left was also used in a different picture of Bianucci et al., unpublished. Image credit: Luisa Quaglia.

Fig. S4. Map of the excavation area (*Left*) showing the location of skeleton OSL1/SZ14604 (*Right*). The map was made by the Norwegian Institute for Cultural Heritage Research (NIKU), using the geographic coordinate system: EUREF89/UTM32. Image credit: Reidar Meyer (NIKU).

Published under the [PNAS license](#).

First published May 26, 2020.

www.pnas.org/cgi/doi/10.1073/pnas.2007983117

Integrative approach using *Yersinia pestis* genomes to revisit the historical landscape of plague during the Medieval Period

Amine Namouchi^{a,1}, Meriam Guellil^{a,2}, Oliver Kersten^{a,2}, Stephanie Hänsch^{a,2}, Claudio Ottoni^a, Boris V. Schmid^a, Elsa Pacciani^b, Luisa Quaglia^b, Marco Vermunt^c, Egil L. Bauer^d, Michael Derrick^d, Anne Ø. Jensen^d, Sacha Kacki^{e,f}, Samuel K. Cohn Jr.^g, Nils C. Stenseth^{a,h,1}, and Barbara Bramanti^{a,i,1}

^aCentre for Ecological and Evolutionary Synthesis (CEES), Department of Biosciences, University of Oslo, N-0316 Oslo, Norway; ^bSoprintendenza Archeologia, Belle Arti e Paesaggio di Firenze, Pistoia e Prato, 50125 Florence, Italy; ^cDepartment of Monuments and Archaeology, Municipality of Bergen op Zoom, 4611BT-59 Bergen op Zoom, The Netherlands; ^dNorwegian Institute for Cultural Heritage Research, N-0155 Oslo, Norway; ^eDepartment of Archaeology, Durham University, DH1 3LE Durham, United Kingdom; ^fUMR 5199 De la Préhistoire à l'Actuel: Culture, Environnement et Anthropologie, Centre National de la Recherche Scientifique, University of Bordeaux, 33615 Pessac, France; ^gSchool of Humanities, University of Glasgow, G12 8QQ Glasgow, United Kingdom; ^hKey Laboratory for Earth System Modeling, Department of Earth System Science, Tsinghua University, Ministry of Education, 100084 Beijing, China; and ⁱDepartment of Biomedical and Specialty Surgical Sciences, Faculty of Medicine, Pharmacy, and Prevention, University of Ferrara, 35-441221 Ferrara, Italy

Contributed by Nils C. Stenseth, October 19, 2018 (sent for review July 26, 2018; reviewed by Bruce M. S. Campbell and Ludovic Orlando)

Over the last few years, genomic studies on *Yersinia pestis*, the causative agent of all known plague epidemics, have considerably increased in numbers, spanning a period of about 5,000 y. Nonetheless, questions concerning historical reservoirs and routes of transmission remain open. Here, we present and describe five genomes from the second half of the 14th century and reconstruct the evolutionary history of *Y. pestis* by reanalyzing previously published genomes and by building a comprehensive phylogeny focused on strains attributed to the Second Plague Pandemic (14th to 18th century). Corroborated by historical and ecological evidence, the presented phylogeny, which includes our *Y. pestis* genomes, could support the hypothesis of an entry of plague into Western European ports through distinct waves of introduction during the Medieval Period, possibly by means of fur trade routes, as well as the recirculation of plague within the human population via trade routes and human movement.

plague | Medieval | ancient DNA | *Yersinia pestis* | Second Pandemic

The Second Plague Pandemic started in the mid-14th century and lasted until the 19th century (1, 2). Its beginning in Europe is marked by a major epidemic event commonly referred to as the Black Death (1346–1353), which ultimately led to the death of at least 30% of the European population (3). The Black Death reached Western Europe in October 1347 through infected Genoese galleys arriving from Caffa (4) and spread over multiple routes and directions, after having reached the thriving trade center of Constantinople (5). Two other pandemics are historically attested, the first, starting in 541–542 CE with the Justinian Plague and lasting in Europe until the mid of the eighth century, and the third, which originated in 1772 in the Yunnan Province, southwest China, and is still ongoing (2, 6).

Plague is a zoonosis, which occasionally spills over to human populations. However, it is primarily a disease of wildlife and is maintained in reservoirs, which nowadays are present on all continents, with the exception of Australia and Western Europe (2, 6). While our knowledge of modern plague reservoirs and their hosts is extensive, it remains unclear which plague reservoir(s) was the origin of the epidemics recorded in Europe throughout its history. Consequently, we are also lacking knowledge of the main routes and mechanisms of transmission during the historical pandemics. Two scenarios have been suggested in previous studies: (i) After a first introduction during the Black Death, plague periodically spilled over from one or more reservoirs located in Western Europe, from where it was later (re)introduced to China and gave rise to the Third Pandemic (7–9); (ii) plague was repeatedly introduced to Western

Europe from a reservoir located in Eastern Europe/Central Asia (1, 2, 10) and spread via commercial trade routes and human movement (11, 12). These two scenarios are mutually exclusive regarding the establishment of local European reservoir of plague during the Second Pandemic.

In this study, we provide five sequenced ancient genomes recovered from four archeological sites: Abbadia San Salvatore (BSS) (Italy), Saint-Laurent-de-la-Cabrerisse (SLC) (France), Bergen op Zoom (BER) (The Netherlands), and Oslo (OSL) (Norway) (Fig. 1). The presented genomes all date to the 14th century and represent the focus of our analysis. By supplying additional genomic data of ancient strains recovered from victims of historical epidemics, our

Significance

While our knowledge of modern plague reservoirs and their hosts is extensive, we have little to no knowledge about the origin of the Medieval plague pandemics or the routes of transmission involved in their spread. Prior genomic data provide a patchy low-resolution picture of the transmission dynamics involved during the Second Plague Pandemic, with only five distinct genomes. We have reevaluated all Medieval strains under the light of archaeological and historical evidence to carefully discuss the involvement of different transmission routes during the Second Plague Pandemic. Our interpretation showcases the importance of trade routes and human movements and further supports the identification of *Yersinia pestis* as the pathogenic agent of the so-called *pestis secunda* (1357–1366).

Author contributions: A.N., S.H., N.C.S., and B.B. designed research; A.N., M.G., O.K., S.H., C.O., and S.K.C. performed research; E.P., L.Q., M.V., E.L.B., M.D., A.Ø.J., and S.K. contributed samples; B.V.S., E.P., L.Q., M.V., E.L.B., M.D., A.Ø.J., S.K., S.K.C., and B.B. provided advice; A.N., M.G., O.K., S.H., and C.O. analyzed data; A.N., M.G., O.K., N.C.S., and B.B. wrote the paper with contributions of all authors; and S.H., C.O., B.V.S., M.V., and S.K.C. edited versions of the paper.

Reviewers: B.M.S.C., The Queen's University of Belfast; and L.O., Natural History Museum of Denmark and University of Copenhagen.

The authors declare no conflict of interest.

This open access article is distributed under Creative Commons Attribution-NonCommercial-NoDerivatives License 4.0 (CC BY-NC-ND).

Data deposition: Raw sequencing reads have been deposited in the European Nucleotide Archive (ENA) (accession no. PRJEB24499).

¹To whom correspondence may be addressed. Email: amine.namouchi@ibv.uio.no, n.c.stenseth@ibv.uio.no, or barbara.bramanti@ibv.uio.no.

²M.G., O.K., and S.H. contributed equally to this work.

This article contains supporting information online at www.pnas.org/lookup/suppl/doi:10.1073/pnas.1812865115/-DCSupplemental.



Fig. 1. Geographic locations of previously and presently described ancient genomes. Map of previously and presently described ancient genomes. The red circles represent the locations of previously described ancient genomes. Yellow circles represent ancient genomes described in this study. For the newly described ancient genomes, the indicated years are discussed in *Results* and *Discussion*. Numbers in parentheses indicate number of ancient genomes included from each site.

study can improve the resolution of the *Yersinia pestis* phylogeny and can contribute to the discussion on transmission routes and reservoir establishments during historical pandemics. Using state-of-the-art bioinformatics methods, we evaluated the evolutionary history of *Y. pestis* by incorporating the data reported in this study into a revised phylogeny. We evaluated our results in light of historical, epidemiological, and ecological studies to improve our understanding of the fully documented spectrum of the dynamics at work during the early decades of the Second Plague Pandemic.

Results

Screening and Authentication of *Y. pestis* DNA in Human Skeletons.

The presence of *Y. pestis* in the samples from Saint-Laurent-de-la-Cabrerisse (SLC) and Bergen op Zoom (BER) has been confirmed by PCR in a previous study by Haensch et al. (13). A similar approach was used to screen 36 individuals from Abbadia San Salvatore (BSS) and nine individuals from Oslo (OSL) (see *Methods* for more details on the experimental work). Positive samples from Abbadia San Salvatore and Oslo were enriched without initial metagenomic screening.

Genomic Data Analyses. We systematically reanalyzed all available raw sequencing data from ancient *Y. pestis* metagenomic datasets from the Second Plague Pandemic. Additionally, we reanalyzed the raw data from two Bronze Age samples and two Justinian

Plague samples from the First Plague Pandemic. Most sequencing data stemming from modern samples were included as well. By systematically reanalyzing the available raw data, we were able to avoid any incongruity caused by differences in data filtering and SNP calling. Our custom data workflow (*SI Appendix, Fig. S5*) also accounted for deamination damage patterns typical for ancient DNA (aDNA). For all generated ancient genomes, reads mapping to the genome of *Y. pestis*, strain CO92, showed a mean read length between 50 and 60 bp, which is consistent with aDNA. The aligned reads also showed a clear deamination profile typical of aDNA misincorporations (*SI Appendix, Fig. S6*). Moreover, by aligning all generated reads from each sample to *Yersinia pseudotuberculosis*, strain IP-32953, the edit distance analysis clearly showed that the reads belong to *Y. pestis* rather than to *Y. pseudotuberculosis* (*SI Appendix, Fig. S7*). In fact, for all aDNA reported in this study, the percentage of reads with an edit distance of 0 is higher when aligned against *Y. pestis* vs. *Y. pseudotuberculosis*.

After read quality rescaling, the transitions to transversion ratios of all aDNA assemblies were comparable with those of modern genomes (*SI Appendix, Fig. S8*), which emphasizes the consistency of our methods and data. In addition, to investigate possible cross-contamination or multiple infection, for each sample, the heterozygous profile analysis (*SI Appendix, Fig. S9 and Table S4*) showed that, for almost all ancient samples, the

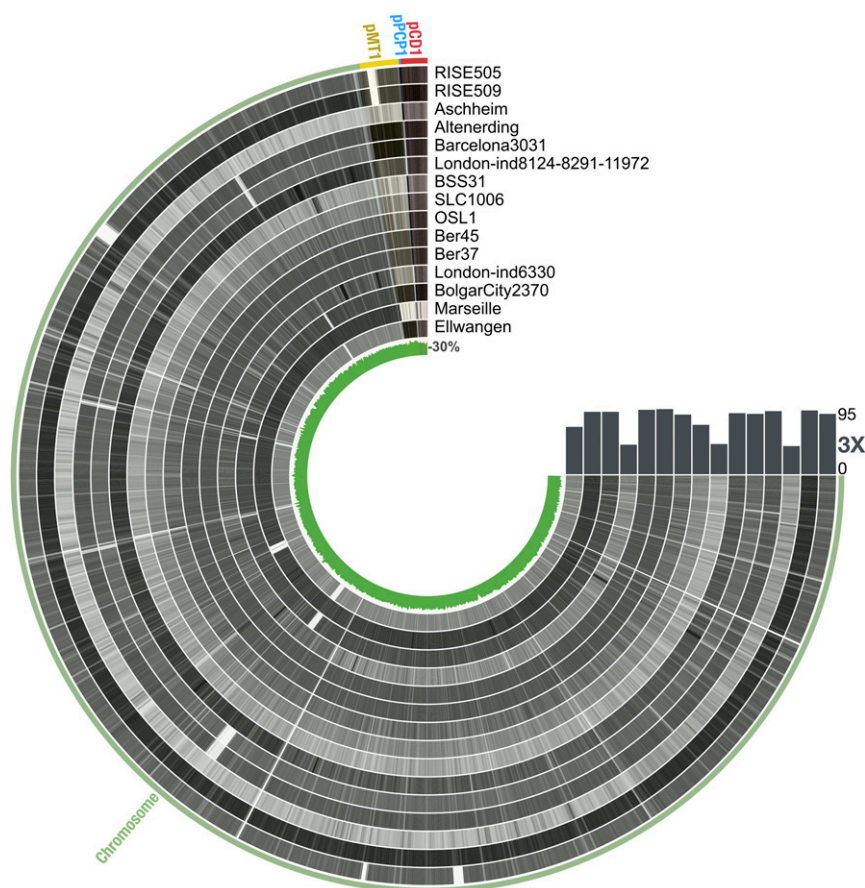


Fig. 2. Overview of the coverage of ancient *Y. pestis* genomes. Each ring corresponds to one ancient genome. The color intensity is proportional to the coverage across the chromosomal genome and plasmids. The coverage rate, as well as the GC content, was measured throughout the genome using a window size of 200 bp. The bars indicate the fraction of the genome with a depth of coverage of 3x. This figure was generated using anvio (69).

heterozygous ratio is low (<0.3), as for modern data. Nevertheless, this ratio is high (>0.4) in some modern data.

The samples from Bergen op Zoom, Ber37 and Ber45, and the sample from Oslo, OSL1, covered more than 87% of the reference genome, with a minimum of 3x depth of coverage (Fig. 2 and *SI Appendix, Table S3*). For the samples SLC1006 (Saint-Laurent-de-la-Cabrerisse) and BSS31 (Abbadia San Salvatore), we were able to recover 73% and 44% of the genome at 3x depth of coverage, respectively (Fig. 2 and *SI Appendix, Table S3*).

Overall, after having considered all possible patterns of deamination derived from diagenetic processes, along with sequencing inconsistencies, and having rescaled the data accordingly, the comparison of 126 modern *Y. pestis* genomes with 15 ancient genomes from the Bronze Age and the First and the Second Pandemic (*SI Appendix, Table S1*) yielded 2,826 polymorphic sites (*SI Appendix, Table S5*). These SNPs were grouped as follows: 1,456 nonsynonymous SNPs, 625 synonymous SNPs, and 745 intergenic SNPs. Among the 2,826 identified polymorphic sites, 112 were homoplastic (3.9%) (*SI Appendix, Table S6*).

Dating of the *Y. pestis* Strain from Abbadia San Salvatore. Attributed to a major epidemic of the second half of the 14th century by archaeological and stratigraphic evidence, the age of the mass grave found at Abbadia San Salvatore (*SI Appendix*), as well as the *Y. pestis* genome retrieved, needed to be refined to help with the interpretation of the phylogenetic tree. The consultation of notarial records from the region, with an impressive increase of death-bed testaments and a decrease of nontestamentary property contracts, revealed the presence of a major dramatic event

from late June to early September 1348 (*SI Appendix, Fig. S3 and Table S2*). The analysis of the data confidently demonstrated that such a catastrophic event, which has no equivalent in the course of the century, was responsible for the death of the large number of victims retrieved in Abbadia San Salvatore.

Evolutionary History Reconstruction. We built our phylogenetic tree using maximum likelihood, as implemented in IQ-TREE (version 1.5.5) (14). *Yersinia pseudotuberculosis*, strain IP32953, was used as an outgroup. The adequate substitution model was identified and applied using ModelFinder (15) before building the phylogeny. After testing 484 models, the best-fitting model, according to the Bayesian information criteria (BIC), was the general time reversible (GTR) model (16), with unequal rates and base frequencies with ascertainment (ASC) bias correction and free rate heterogeneity across sites with four rate categories.

The topology of the generated tree (Fig. 3 and *SI Appendix, Fig. S10*) was supported by three different tests (bootstrap, SH-aLrt, and local bootstrap probability test) and showed a star-like radiation at the end of branch 0, giving rise to branches 1, 2, 3, and 4. As previously reported, two Bronze Age samples from Bateni and Kytmanovo (Russia) (17), as well as the Justinian samples (9, 18), can be found on branch 0 (Fig. 3A). As expected, the five described ancient genomes cluster with all other known Second Plague Pandemic genomes (Fig. 3).

Divergence Dates and Tip Dating. The reconstructed maximum likelihood tree shows a high correlation between the root-to-tip distance and the sampling time (correlation coefficient $r^2 = 0.74$).

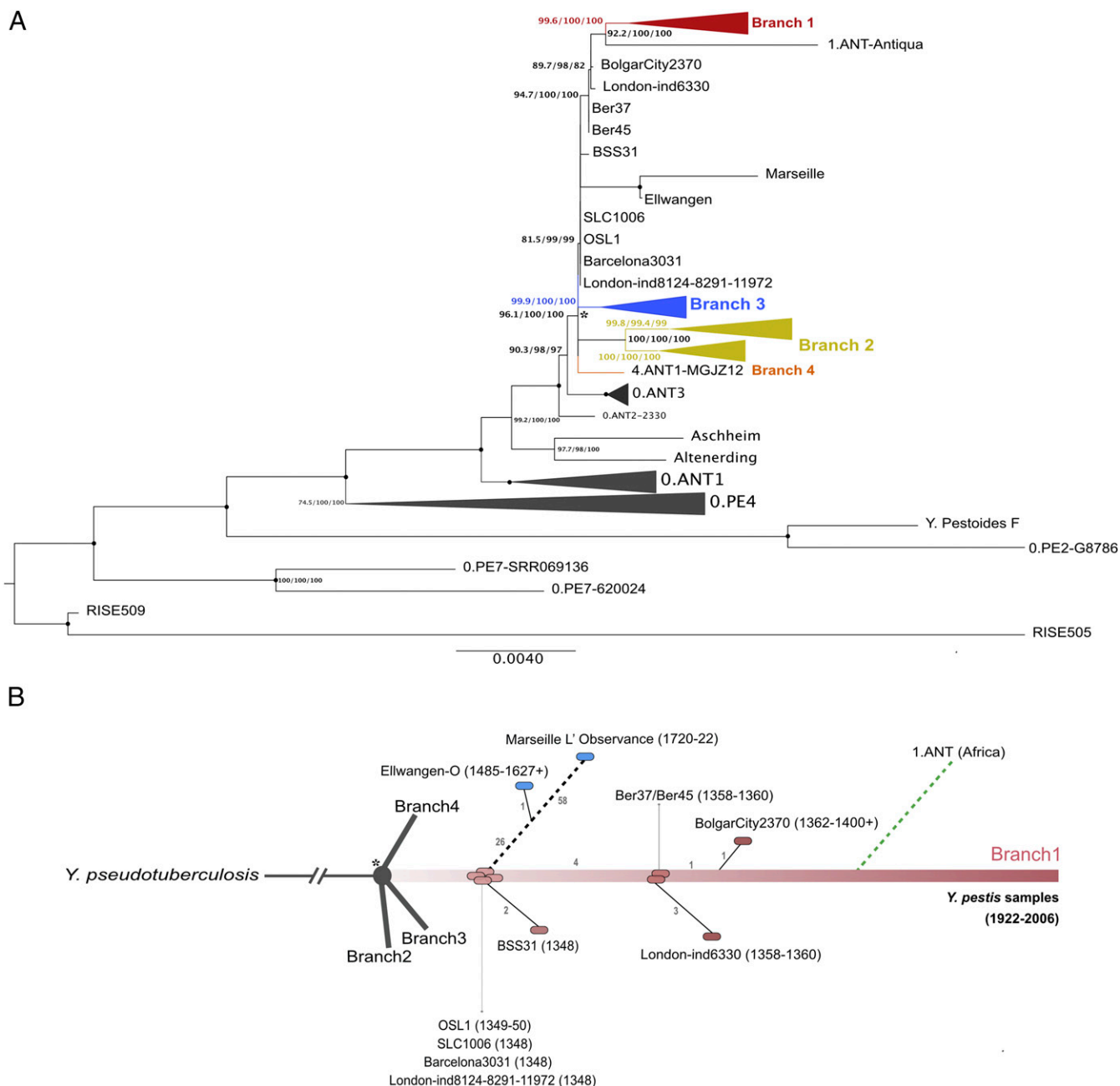


Fig. 3. Reconstruction of the phylogenetic tree and evolutionary history of *Y. pestis*. (A) Maximum likelihood (ML) phylogenetic tree for *Y. pestis*. Consisting of 126 modern *Y. pestis* strains and 15 ancient genomes, the tree was built using IQ-Tree (version 1.5.5) (14), which implements ModelFinder (15) to find the right substitution model before ML tree search. A total number of 2,826 polymorphic sites were used to construct the ML tree, which was visualized and edited using FigTree (version 1.2.1). Strains belonging to branch 1, branch 2, and branch 3 were collapsed for clarity. The numbers at each node indicate the bootstrap values at 1,000 replicates, SH-aLrt support values at 1,000 replicates, and local bootstrap support values, respectively. The nodes indicated by black circles correspond to 100/100/100 of the support values in the same order as previously described. The asterisk marks the polytomy known as the “Big Bang.” (B) Schematic representation of the evolutionary history of *Y. pestis* genomes dated to the Second Plague Pandemic. Each circle represents one sample. The numbers on each branch correspond to the number of sequentially accumulated SNPs (*SI Appendix*).

The date-randomization test (DRT) showed a different result. In fact, the outcome of the DRT showed that the 95% highest posterior density (HPD) of the substitution rate estimated for both the original and 20 date-randomized datasets is overlapping (*SI Appendix*, Fig. S11).

Discussion

As mentioned in the Introduction, two scenarios have been proposed in past studies for the persistence of plague during the

Second Plague Pandemic. However, the few currently available ancient *Y. pestis* genomes have proven insufficient to explain the mechanisms underlying the recurrent plague outbreaks in Europe during the Second Plague Pandemic. To provide further insights into the events driving the Second Plague Pandemic and to properly address which of the two proposed scenario has the highest likelihood, we have evaluated the available data along with five sequenced *Y. pestis* strains stemming from four European archaeological sites of the 14th century, using an integrative



Fig. 4. Schematic representation of the connection between the fur trade routes and the spread of plague during the early stage of the Second Plague Pandemic (14th century). This simplified map shows cities strategically situated along the fur trade routes (indicated as a white line). The city of Novgorod (Russia) has played a central role in fur export to cities like Hamburg and Lübeck. The regions highlighted in orange represent known modern plague reservoirs. The darker orange delimits the region in which we believe secondary plague reservoirs were established before the Black Death. The red dots represent the locations of all known ancient *Y. pestis* genomes. Black lines, Silk Road; dark-blue lines, maritime trade routes.

trade routes, a complex network of interconnected maritime, riverine, and overland routes into Western Europe. During the second half of the 14th century, Bolgar and Novgorod (Russia) (Fig. 4) had established an economic dominance as major fur trade centers. Fur was historically an important trade good, which was widely commercialized on established itineraries all over Eurasia. Starting with the second half of the 13th century, Novgorod had gained access to the Western European markets through the Hanseatic League, which it eventually became part of (35). The flourishing of the League in the 14th century permitted Novgorod to export big consignments of fur to London via Lübeck and Hamburg (35, 38). Thus, the three specific SNPs found in London-ind6330 might have been acquired over the course of a more complex transmission chain, similar to Abbadia San Salvatore (Fig. 3B), since the territories of the Hanseatic League were also affected by plague during the *pestis secunda* (39). However, as plague also struck many Mediterranean ports between 1357 and 1361 (e.g., Alexandria in 1357–1358 and 1361, Venice in 1359–1361, Genoa in 1360–1361, and Ragusa/Dubrovnik in 1361 and Constantinople) (40), it becomes difficult to determine precisely the point of entry and the routes of transmission of the *pestis secunda* (40). However, a reintroduction from outside seems most likely both from historical (5) and climatic (10) evidence.

On the other hand, the Black Death in Western Europe may also be due to importations on the fur trade network. During the 14th century, Russia was under the domination of the Golden Horde, which had imposed new regulations on the fur trade, and merchants from Bolgar had started importing their fur from the “Land of Darkness,” a region speculated to be situated on the Kama river (41). After exporting it to Sarai (Southern Volga region), which is placed in the easternmost part of Europe, fur was distributed to all parts of Eurasia along with other goods. Remarkably, in the 1340s, there was a significant change that impacted the routes of the fur trade. In fact, a new mainland route connecting Sarai, Tana, and Caffa had been established with the support of the Golden Horde. Traded goods were then further exported from Caffa on the Black Sea trading network by the Genoese (41). Historians have remarked that a considerable variety of fur had started to appear in the ports of the Black Sea by the 1340s (41). These events seem to coincide chronologically

with the onset of the Black Death, whose origins remain unclear before its arrival from Caffa. Suggestively, Ibn al-Wardī, an Arab historian, who died of plague in Aleppo (Syria) in 1349, described how returning merchants from Crimea, attributed the beginning of the “contagion” to the “Land of Darkness,” in which the pestilence had been present for 15 years before reaching the West (3). Without having visited the West-Ural region from which fur was imported to the Volga centers, the Arab merchants likely just meant that the source of the Black Death was associated with the fur routes, placed somewhere before Sarai (seen from Caffa), where plague was present before 1347 (3), and hence probably a region next to the Caspian Sea—an area with well-established plague reservoirs today (Fig. 4). From this region, plague may have been transported on the fur trade network to the whole of Europe, not only during the Black Death, but also later, with (possibly) independent goods deliveries to Bergen op Zoom, London, and Bolgar. Extra-SNPs, which developed on subbranches lateral to branch 1, might also have been accumulated during chains of epidemics on the long journey to Western Europe.

Overall, evidence from different disciplines increasingly suggests successive and independent introductions of plague to Western Europe via the transport of infected individuals and goods on trade routes during the Second Plague Pandemic. By analyzing five ancient genomes from the Second Plague Pandemic, adding them to the established *Y. pestis* phylogeny, and evaluating them with a historical background, our study aimed to answer some of the most debated questions on plague in Western Europe during the Second Plague Pandemic. All things considered, the hypothesis that *Y. pestis* reached Europe through multiple introductions during the Middle Ages through different routes, including the fur trade, appears very plausible, at least during the Second Plague Pandemic.

Methods

Samples. The *Y. pestis* strains presented in this study stem from four European sites dating to the second half of the 14th century (Fig. 1): Saint-Laurent-de-la-Cabrerisse (France) (13), Bergen op Zoom (The Netherlands) (13), Oslo (Norway) (42), and Abbadia San Salvatore (Italy).

For this study, a total of 126 *Y. pestis* strains (SI Appendix, Table S1) and 15 published ancient DNA samples were used, including 2 Bronze Age samples (17), 2 Justinian plague samples (9, 43), and 10 samples from the Second Plague Pandemic (7, 19).

Dating the Strain of Abbadia San Salvatore with Historical Data. We collected data of testaments and contracts from 1340 to 1381 (SI Appendix, Fig. S3 and Table S2), a period followed by a gap in documentation until 1440, as documented in inventories (available for consultation at the Archivio di Stato, Florence, Italy), which summarize parchments from Monte Amiata, the region where Abbadia San Salvatore is placed.

Sample Preparation. We screened a total of 6 teeth from the site of Saint-Laurent-de-la-Cabrerisse, 41 teeth from the site of Abbadia San Salvatore, 3 teeth from the site of Bergen op Zoom, and 18 teeth from the site of Oslo. Laboratory work was performed at the Paleogenetics Laboratories at the University of Mainz, (Germany) and at the Ancient DNA Laboratory at the University of Oslo (Norway). Both laboratories are solely dedicated to the analysis of ancient samples and are subjected to strict anticontamination protocols, including full overnight UV irradiation. Target enrichment was performed at the post-PCR capture laboratory of the Centre for Ecological and Evolutionary Synthesis (CEES), University of Oslo, Oslo.

Extraction and PCR Screening. The teeth were decontaminated, sandblasted, and milled to fine powder, as previously described (13). aDNA was extracted using either a previously published phenol chloroform protocol (13) or modified versions of silica-based protocols based on Brotherton et al. (44) or Dabney et al. (45). We used 0.2 to 0.5 g of tooth powder for phenol chloroform extractions and 0.1 to 0.26 g for the silica-based extraction methods. Two samples from Bergen op Zoom (Ber37 and Ber45), 6 samples from Saint-Laurent-de-la-Cabrerisse, and 39 samples from Abbadia San Salvatore were extracted by phenol chloroform extraction (protocol A) (SI Appendix). Three teeth from Saint-Laurent-de-la-Cabrerisse, 2 teeth from Abbadia San

Salvatore, and 18 teeth from Oslo were extracted via silica extraction based on Brotherton et al. (44) (protocol B) (*SI Appendix*). Lastly, one tooth from Abbadia San Salvatore was extracted using a protocol based on Dabney et al. (45) (protocol C) (*SI Appendix*). All extractions included negative milling and extraction controls.

All extracts, which had not previously been screened for *Y. pestis* in Haensch et al. (13), were screened for human and *Y. pestis* DNA using previously published primers: pla YP11D/YP10R as published in Raoult et al. (46), caf1 caf1U2/L2 as published in Haensch et al. (13), and human mitochondrial HVR1 primers L16209 (47) and H16348 (48). PCR conditions were as described in Haensch et al. (13). Positive samples were shotgun sequenced on an Illumina HiSeq2500 system [125 bp paired end (PE)] at the Norwegian Sequencing Centre (NSC) at the University of Oslo.

Library Preparation and Target Enrichment. Library preparation was done following a modified Meyer and Kircher (49) protocol (for more details, see *SI Appendix*). Amplified libraries were purified using commercial kits (Stratagene PCRapace or Qiagen MinElute PCR purification kits, followed by an AMPureXP beads purification) and subsequently quantified on a Bioanalyzer 2100 expert dsDNA High Sensitivity Chip and using a Qubit HS assay kit. When necessary, reamplifications were performed with IS5 and IS6 primers following the original protocol by Meyer and Kircher (49). Positive samples, screened via standard PCR and/or shotgun metagenomics, were enriched for *Y. pestis* DNA. Over the course of this study, we used two different custom bait kits from different manufacturers for in-solution target enrichment (for more details, see *SI Appendix*).

Sequencing. High throughput sequencing (125 bp PE) of the captured libraries was performed on an Illumina HiSeq2500 system at the NSC (University of Oslo). Capture products from Ber45 were pooled on one lane, SLC1006 products were split over two lanes (single capture and double capture products were sequenced separately), and Bss 31d and Ber37c products were each sequenced and pooled with other samples on different lanes and flow cells. Libraries for OSL1A were sequenced and multiplexed with other libraries over two lanes.

Shotgun Metagenomics Data Analysis. The presence of *Y. pestis* in shotgun metagenomic datasets was investigated using two methods. The first method is based on read abundance of specific genes and was implemented in Metaphlan (50). The second method is based on the exact alignments of k-mers and was implemented in Kraken (51). This procedure was only applied when the first screening using qPCR was ambiguous.

Mapping-Based SNP Analysis. We designed a custom pipeline (*SI Appendix, Fig. S5*) to analyze raw sequencing data from modern and ancient genomes using snakemake as the workflow manager system (52). The genome of the *Y. pestis* strain CO92 was used as reference. Paired-end reads in fastq format were trimmed and merged using ClipAndMerge (<https://github.com/apeltzer/ClipAndMerge>). Thereafter, we used bwa-aln (53) to align the merged reads against *Y. pestis* strain CO92 by disabling the seed option (-l) and setting the option -n to 0.1 (for modern data, the -n option was set to 0.01). Duplicated reads were identified and marked using picard-tools (broadinstitute.github.io/picard/). Local alignment of reads was performed around gapped regions before SNP calling using the GATK IndelRealigner module (<https://software.broadinstitute.org/gatk/>). DeDup (<https://github.com/apeltzer/DeDup>) was also used to remove duplicated sequences as it has been specifically designed for merged reads. Aligned Binary Alignment Map (BAM) files of ancient DNA samples were analyzed using MapDamage2 (54) to assess and recalibrate aDNA damage patterns in the form of C-to-T or G-to-A conversions.

Edit Distance. To verify that the generated reads belong to *Y. pestis* rather than *Y. pseudotuberculosis*, all reads from each sample were mapped to the genome of *Y. pseudotuberculosis*, strain IP-32953, as described above. The edit distance, which defines the minimal number of substitutions, insertions, and deletions to transform the read sequence to its homologous sequence in

the reference genome, was calculated using BAMStats (bamstats.sourceforge.net/).

SNPs Call. SNP calling was performed using samtools (55, 56) and bcftools (<https://samtools.github.io/bcftools/>). SNPs located within a frame of 10 bp from indels were excluded with samtools. For each sample, all identified SNPs were filtered and annotated using a freely available tool, snpToolkit (<https://bitbucket.org/Amine-Namouchi/snpToolkit>); snpToolkit allows one to filter and annotate SNPs from vcf files by providing the genbank file of the reference sequence used during reads alignment. SNPs were filtered according to three criteria: quality score (≥ 30), depth of coverage (≥ 3), and allele frequency (90%). In addition, SNPs that are close to each other by less than 10 bp were excluded during the annotation process using snpToolkit with option -f. All generated annotation output files were thereafter compared against each other using the snpToolkit option combine. For each polymorphic site, snpToolkit checks the corresponding alignment region in the bam file to accurately determine the distribution of each polymorphic site by considering the same region in all other aDNA strains of the Second Plague Pandemic. The efficiency of the method implemented in snpToolkit was assessed after manual inspection of these polymorphic sites using Integrative Genomics Viewer (IGV) (57, 58). The option combine produces two output files. The first one represents the distribution of all identified polymorphic sites of all analyzed samples. The second file is a concatenation of all polymorphic sites in fasta format.

Phylogenetic Analysis. Phylogenies were inferred using IQ-TREE (14). IQ-TREE was run using ModelFinder (15), with the option -m MFP to infer the best substitution model for building the maximum likelihood phylogenetic tree. A total number of 484 models were tested. One thousand fast bootstrap replicates were performed to assess statistical support (59). In addition, branch supports were also assessed through the single branch test SH-aLRT (60) with 1,000 replicated as well as local bootstrap probability tests (61). As the concatenated SNPs include missing information indicated by an exclamation mark in the fasta file generated using snpToolkit, we also used the ASC option to account for ascertainment bias correction. The generated tree was visualized using FigTree (version 1.2.1, tree.bio.ed.ac.uk/software/figtree/), and the substitutions leading to each SNP were mapped in the phylogenetic tree using Fastml v3.1 (62).

Divergence Time and Tip Dating Analysis. Temporal signal detection in the sequence data was performed using TempEst (63). As previously described (17, 64, 65), the lognormal relaxed clock model and constant population size models implemented in BEAST (66) were applied to the alignment sequence and phylogenetic tree to determine the divergence dates at each node. To evaluate the reliability of the Bayesian inference, we applied the date-randomization test (DRT) as implemented in the R package tipdatingbeast (67) to generate 20 BEAST input files in xml format with randomized dates. As the out dataset included a large number of modern sequences, the randomization process was only applied to ancient sequences, as previously recommended (68). BEAST was run on each file for 50 million iterations.

Data Availability. Raw sequencing reads produced for this study have been deposited in the European Nucleotide Archive (ENA) under accession number ENA: PRJEB24499.

ACKNOWLEDGMENTS. We thank Lars Walløe for useful comments and discussion; and Joachim Burger for providing access to the aDNA facilities at the University of Mainz, Germany. This project was funded by the European Research Council (ERC) under the FP7-IDEAS-ERC Program (Grant 324249). Part of the data analysis was performed on the Abel Cluster, owned by the University of Oslo and the Norwegian metacenter for High Performance Computing (NOTUR) and operated by the Department for Research Computing at the University Center for Information Technology Services (USIT), University of Oslo. C.O. is funded by Satsningsmiljø Grant Comparative Infection Biology (COMPI), Department of Biosciences, University of Oslo.

- Stenseth NC, et al. (2008) Plague: Past, present, and future. *PLoS Med* 5:e13.
- Bramanti B, Stenseth NC, Walløe L, Lei X (2016) Plague: A disease which changed the path of human civilization. *Adv Exp Med Biol* 918:1–26.
- Benedictow OJ (2004) *The Black Death 1346-1353: The Complete History* (Boydell Press, Woodbridge, UK).
- Michele da Piazza (1980) *Cronaca*, ed Giuffrida A (ILA Palma, Palermo, Italy).
- Campbell BMS (2016) *The Great Transition: Climate, Disease and Society in the Late-Medieval World* (Cambridge Univ Press, Cambridge, UK).
- Vogler AJ, et al. (2013) A decade of plague in Mahajanga, Madagascar: Insights into the global maritime spread of pandemic plague. *MBio* 4:e00623-12.

- Spyrou MA, et al. (2016) Historical *Y. pestis* genomes reveal the European Black Death as the source of ancient and modern plague pandemics. *Cell Host Microbe* 19:874–881.
- Bos KI, et al. (2011) A draft genome of *Yersinia pestis* from victims of the Black Death. *Nature* 478:506–510.
- Wagner DM, et al. (2014) *Yersinia pestis* and the plague of Justinian 541-543 AD: A genomic analysis. *Lancet Infect Dis* 14:319–326.
- Schmid BV, et al. (2015) Climate-driven introduction of the Black Death and successive plague reintroductions into Europe. *Proc Natl Acad Sci USA* 112:3020–3025.
- Yue RPH, Lee HF, Wu CYH (2016) Navigable rivers facilitated the spread and recurrence of plague in pre-industrial Europe. *Sci Rep* 6:34867.

12. Yue RPH, Lee HF, Wu CYH (2017) Trade routes and plague transmission in pre-industrial Europe. *Sci Rep* 7:12973.
13. Haensch S, et al. (2010) Distinct clones of *Yersinia pestis* caused the Black Death. *PLoS Pathog* 6:e1001134.
14. Nguyen L-T, Schmidt HA, von Haeseler A, Minh BQ (2015) IQ-TREE: A fast and effective stochastic algorithm for estimating maximum-likelihood phylogenies. *Mol Biol Evol* 32:268–274.
15. Kalyaanamoorthy S, Minh BQ, Wong TKF, von Haeseler A, Jermini LS (2017) ModelFinder: Fast model selection for accurate phylogenetic estimates. *Nat Methods* 14:587–589.
16. Tavaré S (1986) Some probabilistic and statistical problems in the analysis of DNA sequences. *American Mathematical Society: Lectures on Mathematics in the Life Sciences* (American Mathematical Society, Fort Collins, CO), Vol 17, pp 57–86.
17. Rasmussen S, et al. (2015) Early divergent strains of *Yersinia pestis* in Eurasia 5,000 years ago. *Cell* 163:571–582.
18. Harbeck M, et al. (2013) *Yersinia pestis* DNA from skeletal remains from the 6(th) century AD reveals insights into Justinianic plague. *PLoS Pathog* 9:e1003349.
19. Bos KI, et al. (2016) Eighteenth century *Yersinia pestis* genomes reveal the long-term persistence of an historical plague focus. *eLife* 5:e12994.
20. Kacki S, Rahalison L, Rajerison M, Ferroglio E, Bianucci R (2011) Black Death in the rural cemetery of Saint-Laurent-de-la-Cabrerisse Aude-Languedoc, southern France, 14th century: Immunological evidence. *J Archaeol Sci* 38:581–587.
21. Hirsch A (1881) *Handbuch der Historisch-Geographischen Pathologie* (Stuttgart Enke, Stuttgart, Germany).
22. Walløe L (1982) Pest og folketall 1350–1750 [Plague and Population: Norway 1350–1750]. *Historisk Tidsskrift (Norge)* 61:1–45. Norwegian.
23. Oeding P (1990) [The Black Death in Norway]. *Tidsskr Nor Laegeforen* 110:2204–2208. Norwegian.
24. Brothen JA (1996) Population decline and plague in late medieval Norway. *Ann Demogr Hist (Paris)*, 137–149.
25. Benedictow OJ (2016) *The Black Death and Later Plague Epidemics in the Scandinavian Countries: Perspectives and Controversies* (Sciend, Warsaw).
26. Cohn SK, Jr (2018) *Epidemics: Hate and Compassion from the Plague of Athens to AIDS* (Oxford Univ Press, Oxford).
27. Bowsky WM (1964) The impact of the Black Death upon Sienese government and society. *Speculum* 39:1–34.
28. Carmichael AG (2016) Plague Persistence in Western Europe: A Hypothesis. *The Medieval Globe: Vol 1, No 1, Article 8*.
29. Russell P (1791) *A Treatise of the Plague: Containing an Historical Journal, and Medical Account, of the Plague, at Aleppo, in the Years 1760, 1761, and 1762* (G.G.J. and J. Robinson, London).
30. Devaux CA (2013) Small oversights that led to the Great Plague of Marseille (1720–1723): Lessons from the past. *Infect Genet Evol* 14:169–185.
31. Simpson WJ (2010) *A Treatise on Plague: Dealing with the Historical, Epidemiological, Clinical, Therapeutic and Preventive Aspects of the Disease* (Cambridge Univ Press, Cambridge, UK).
32. Wheelis M (2002) Biological warfare at the 1346 siege of Caffa. *Emerg Infect Dis* 8: 971–975.
33. Ditrich H (2017) The transmission of the Black Death to western Europe: A critical review of the existing evidence. *Mediterr Hist Rev* 32:25–39.
34. Curtis DR, Roosen J (2017) The sex-selective impact of the Black Death and recurring plagues in the Southern Netherlands, 1349–1450. *Am J Phys Anthropol* 164:246–259.
35. Donald Ostrowski MTP (2011) *Portraits of Old Russia: Imagined Lives of Ordinary People, 1300–1745* (Routledge, London).
36. Коваль ВЮ (2013) Торговый инвентарь из раскопок базара середины XIV века в Болгаре. *Поволжская Археология*. Available at archaeologie.pro/ru/archive/6/97/. Accessed June 11, 2018.
37. Yu KV (2013) Trade stock from excavation the market of the middle of the XIV century at Bolgar. *Volga River Reg Archaeol* 4:9–33.
38. Veale EM (2003) *The English Fur Trade in the Later Middle Ages* (London Record Society, London), 2nd Ed, Vol 38. Available at <https://www.british-history.ac.uk/london-record-soc/vol38>. Accessed July 3, 2018.
39. Suhm PF, Nyerup R (2012) *Historie AF Danmark: Fra AAR 1340 Til 1375* (Nabu Press, Charleston, SC). Available at <https://www.betterworldbooks.com/product/detail/historie-af-danmark-fra-aar-1340-til-1375-volume-13-1274946565>. Accessed July 3, 2018.
40. Varlik N (2015) *Plague and Empire in the Early Modern Mediterranean World: The Ottoman Experience, 1347–1600* (Cambridge Univ Press, Cambridge, UK).
41. Martin J (1978) The Land of Darkness and the Golden Horde. The fur trade under the Mongols XIII–XIVth centuries. *Cah Monde Russe Sov* 19:401–421.
42. Guellil M, et al. (2018) Genomic blueprint of a relapsing fever pathogen in 15th century Scandinavia. *Proc Natl Acad Sci USA* 115:10422–10427.
43. Feldman M, et al. (2016) A high-coverage *Yersinia pestis* genome from a sixth-century Justinianic plague victim. *Mol Biol Evol* 33:2911–2923.
44. Brotherton P, et al.; Genographic Consortium (2013) Neolithic mitochondrial haplogroup H genomes and the genetic origins of Europeans. *Nat Commun* 4:1764.
45. Dabney J, et al. (2013) Complete mitochondrial genome sequence of a Middle Pleistocene cave bear reconstructed from ultrashort DNA fragments. *Proc Natl Acad Sci USA* 110:15758–15763.
46. Raoult D, et al. (2000) Molecular identification by “suicide PCR” of *Yersinia pestis* as the agent of medieval Black Death. *Proc Natl Acad Sci USA* 97:12800–12803.
47. Handt O, Krings M, Ward RH, Pääbo S (1996) The retrieval of ancient human DNA sequences. *Am J Hum Genet* 59:368–376.
48. Haak W, et al. (2005) Ancient DNA from the first European farmers in 7500-year-old Neolithic sites. *Science* 310:1016–1018.
49. Meyer M, Kircher M (2010) Illumina sequencing library preparation for highly multiplexed target capture and sequencing. *Cold Spring Harb Protoc* 2010:db.prot5448.
50. Truong DT, et al. (2015) MetaPhlAn2 for enhanced metagenomic taxonomic profiling. *Nat Methods* 12:902–903.
51. Wood DE, Salzberg SL (2014) Kraken: Ultrafast metagenomic sequence classification using exact alignments. *Genome Biol* 15:R46.
52. Köster J, Rahmann S (2012) Snakemake—A scalable bioinformatics workflow engine. *Bioinformatics* 28:2520–2522.
53. Li H, Durbin R (2009) Fast and accurate short read alignment with Burrows–Wheeler transform. *Bioinformatics* 25:1754–1760.
54. Jónsson H, Ginolhac A, Schubert M, Johnson PLF, Orlando L (2013) mapDamage2.0: Fast approximate Bayesian estimates of ancient DNA damage parameters. *Bioinformatics* 29:1682–1684.
55. Li H, et al.; 1000 Genome Project Data Processing Subgroup (2009) The sequence alignment/map format and SAMtools. *Bioinformatics* 25:2078–2079.
56. Li H (2011) A statistical framework for SNP calling, mutation discovery, association mapping and population genetical parameter estimation from sequencing data. *Bioinformatics* 27:2987–2993.
57. Thorvaldsdóttir H, Robinson JT, Mesirov JP (2013) Integrative genomics viewer (IGV): High-performance genomics data visualization and exploration. *Brief Bioinform* 14: 178–192.
58. Robinson JT, et al. (2011) Integrative genomics viewer. *Nat Biotechnol* 29:24–26.
59. Minh BQ, Nguyen MAT, von Haeseler A (2013) Ultrafast approximation for phylogenetic bootstrap. *Mol Biol Evol* 30:1188–1195.
60. Guindon S, et al. (2010) New algorithms and methods to estimate maximum-likelihood phylogenies: Assessing the performance of PhyML 3.0. *Syst Biol* 59:307–321.
61. Adachi J, Hasegawa M (1996) MOLPHY version 2.3: Programs for molecular phylogenetics based on maximum likelihood. Available at citeseerx.ist.psu.edu/viewdoc/summary?doi=10.1.1.476.8552. Accessed September 5, 2018.
62. Ashkenazy H, et al. (2012) FastML: A web server for probabilistic reconstruction of ancestral sequences. *Nucleic Acids Res* 40:W580–W584.
63. Rambaut A, Lam TT, Max Carvalho L, Pybus OG (2016) Exploring the temporal structure of heterochronous sequences using TempEst (formerly Path-O-Gen). *Virus Evol* 2:vev007.
64. Cui Y, Song Y (2016) Genome and evolution of *Yersinia pestis*. *Yersinia pestis: Retrospective and Perspective*, eds Yang R, Anisimov A (Springer, Dordrecht, The Netherlands), pp 171–192.
65. Andrades Valtueña A, et al. (2017) The stone age plague and its persistence in Eurasia. *Curr Biol* 27:3683–3691.e8.
66. Drummond AJ, Bouckaert RR (2015) *Bayesian Evolutionary Analysis with BEAST 2* (Cambridge Univ Press, Cambridge, UK).
67. Rieux A, Khatchikian CE (2017) tipdatingbeast: An R package to assist the implementation of phylogenetic tip-dating tests using beast. *Mol Ecol Resour* 17: 608–613.
68. Ho SYW, et al. (2011) Bayesian estimation of substitution rates from ancient DNA sequences with low information content. *Syst Biol* 60:366–375.
69. Eren AM, et al. (2015) Anvi'o: An advanced analysis and visualization platform for 'omics data. *PeerJ* 3:e1319.